Density Regimes of Complete Detachment and Serpens Mode in LHD

Junichi MIYAZAWA, Suguru MASUZAKI, Motoshi GOTO, Naoki TAMURA, Ryuichi SAKAMOTO, Byron J. PETERSON, Ichihiro YAMADA, Kazumichi NARIHARA, Kenji TANAKA, Tokihiko TOKUZAWA, Mamoru SHOJI, Hisamichi FUNABA, Satoru SAKAKIBARA, Masahiro KOBAYASHI, Masaki OSAKABE, Shigeru MORITA, Hajime ARIMOTO[1)], Katsumi KONDOH[1)], Sadayoshi MURAKAMI[2)], Masaki NISHIURA, Naoko ASHIKAWA, Tomohiro MORISAKI, Kiyohiko NISHIMURA, Hiroshi YAMADA, Nobuyoshi OHYABU, Akio KOMORI, Osamu MOTOJIMA and the LHD Experimental Group

National Institute for Fusion Science, Toki 509-5292, Japan
[1)]*Graduate School of Energy Science, Kyoto University, Uji 611-0011, Japan*
[2)]*Department of Nuclear Engineering, Kyoto University, Kyoto 606-8501, Japan*

(Received 26 November 2005 / Accepted 10 April 2006)

In the Large Helical Device (LHD), the hot plasma column shrinks at the high-density regime and complete detachment takes place. Hydrogen volume recombination is observed at complete detachment. This phase is self-sustained under specific experimental conditions and called the Serpens mode (self-regulated plasma edge 'neath the last-closed-flux-surface). The Serpens mode is achieved after either rapid or slow density ramp up, and either by hydrogen or helium gas puffing. The threshold conditions for complete detachment and the Serpens mode are experimentally documented in the parameter space of heating power and density. The threshold density for the Serpens mode transition increases with ~ 0.4 power of the heating power. The total radiation is shown to be not adequate to describe the threshold conditions, since it mainly includes the information of very edge region outside the hot plasma column. The operational density limit in LHD, which is sustainable in steady state, has been extended to 1.7 times as high as the Sudo density limit, by applying pellet injection to the Serpens plasmas.

Keywords: high-density plasma, detachment, Serpens mode, serpent, volume recombination, density limit

DOI: 10.1585/pfr.1.026

1. Introduction

In magnetically confined fusion reactors, it is expected that the divertor heat load will exceed $10\,\mathrm{MW/m^2}$, without any effective cooling of divertor heat flux [1–3]. This is unfavorable for realistic divertor target materials especially in steady-state operation. Divertor detachment is effective to reduce the heat load onto the target. In diverted tokamaks, detachment is achieved by increasing the divertor plasma density or by introducing impurities such as neon to enhance the radiation loss [4–7]. Also in a stellarator, W7-AS, the divertor plasma partially detaches from the target at a high-density regime of 3–4 $\times\ 10^{20}\ \mathrm{m^{-3}}$ [8–10]. Near the operational density limit, toroidally axisymmetric radiation belt, called *Marfe*, is often observed in tokamaks [4, 11] and W7-AS [12–14]. In the world largest super-conducting heliotron, Large Helical Device (LHD) [15–18], a Marfe like toroidal radiation belt, which is poloidally asymmetric while toroidally symmetric [19], has been observed at the radiative collapse phase [20, 21]. In this phase, *complete detachment* takes place because the plasma column shrinks, and significant reduction in the divertor flux is observed at all the measured divertor tiles. However, this complete detachment is transient. It has been shown that complete detachment is observed when the minor radius of the effective hot plasma boundary (defined as the radial position where the electron temperature is 100 eV as will be discussed in Sec. 2) becomes smaller than the minor radius of the last-closed-flux-surface (LCFS) [22]. It is possible to recover from shrinking by stopping the gas feed. In some cases, the shrunken hot plasma boundary is quasi-steadily sustained beneath the LCFS, which is called the *Serpens mode* [23]. The Serpens mode is a subset of complete detachment that continues for a period longer than the energy confinement time. During the Serpens mode, the divertor flux (ion saturation current) normalized by the main plasma density decreases to $\sim 10\,\%$ of that during the attached phase [24]. A rotating helical radiation belt named the *serpent* [25] appears in the Serpens mode, which is asymmetric both poloidally and toroidally. The serpent causes fluctuations in edge plasma properties such as the divertor flux, H_α and C_{III} intensities. The energy confinement of Serpens plasmas is evaluated to be comparable to that of the high-

author's e-mail: miyazawa@LHD.nifs.ac.jp

density attached plasmas [24], taking into consideration the shrinking effective plasma minor radius, shallow penetration of heating beams, and the weak temperature dependence of the effective thermal diffusivity that appear in the high-density regime in LHD [26–28].

Although both detachment and confinement properties comparable to the high-density attached plasmas are realized in the Serpens plasmas [24], the most appropriate experimental scenario to achieve the Serpens mode with high reproducibility has not yet been understood. To control the Serpens plasmas, it is necessary to know the key parameters determining the threshold for the Serpens mode transition. In this study, the necessary conditions for the Serpens mode are investigated. Possible influences of the radiation loss, impurity emission, density ramp up rate, gas species are discussed as well as the density and the heating power. Appearance of the Serpens mode marks an operational density limit in LHD, as the Marfe in W7-AS or tokamaks, i.e. the density regime where the Serpens mode appears is located just below the operational density limit. In the next section, typical characteristics of the Serpens mode are described. Necessary conditions to attain the Serpens mode are discussed in Sec. 3. These results are summarized in Sec. 4.

2. Serpens Mode

2.1 Typical waveforms

Typical waveforms of the Serpens mode discharge are depicted by red lines in Fig. 1. Other examples are also shown in the figure; one is a discharge that does not enter the Serpens mode (denoted by "Attached plasma", blue lines) and another is a discharge terminated by radiative collapse ("Collapse", gray lines). In all three cases, the plasmas are initiated by 84 GHz electron cyclotron heating (t = 0.15–0.5 s, not shown) and sustained by negative-ion based neutral beam injection of $P_{\rm NB}^{\rm PT}$ ~ 7–9 MW ($P_{\rm NB}^{\rm PT}$ is the total port-through power). Before t = 1 s, the electron density is feedback controlled by gas puffing and then a short pulse of "massive" gas puff is applied at a rate of $\Phi_{\rm puff}$ ~ 200 Pa m^3/s. The volume averaged electron density, $\langle n_{\rm e}\rangle$, is rapidly increased from the feedback level of $\langle n_{\rm e}\rangle$ ~ 5×10^{19} m^{-3} to $\langle n_{\rm e}\rangle$ ~ 10×10^{19} m^{-3} by the massive gas puffing. It should be noted that an identical massive gas puff is applied for all of three cases. During the feedback phase, on the other hand, $\langle n_{\rm e}\rangle$ in the three cases are slightly different due to recycling, which varies shot to shot depending on the amount of hydrogen atoms loaded on the plasma-facing components in the preceding discharges. Especially in the "Collapse" discharge, $\langle n_{\rm e}\rangle$ at the feedback phase finally reaches ~ 6×10^{19} m^{-3}, even though the $\Phi_{\rm puff}$ is shut off at t ~ 0.6 s. When the recycling is small as in the "Attached plasma" case, $\Phi_{\rm puff}$ at the feedback phase becomes larger. In this case, however, $\langle n_{\rm e}\rangle$ at the feedback phase is slightly smaller than that in the "Serpens mode" case. In Fig. 1 (c), the temporal behavior of the effective hot plasma boundary, $\rho_{100\,\rm eV}$, is depicted. As in the former studies [22–24, 28], $\rho_{100\,\rm eV}$ denotes the normalized minor radius, $\rho = r/a_{\rm LCFS}$, where the electron temperature, $T_{\rm e}$, is 100 ± 50 eV ($a_{\rm LCFS}$ is the minor radius of the LCFS). The measurable range of our Thomson scattering system [29] is $T_{\rm e} \geq 30$ eV. Owing to the steep temperature gradient at ~ $\rho_{100\,\rm eV}$ in typical detached plasmas, where $T_{\rm e}$ increases from 30 to 100 eV within $\delta\rho$ ~ 0.05 [22, 24], the hot plasma boundary at detachment is well approximated by $\rho_{100\,\rm eV}$. Although $\delta\rho$ is ~ 0.1 or larger in attached plasmas, on the other hand, due to the ergodic layer extending outside the LCFS, $\rho_{100\,\rm eV}$ still is representative of the hot plasma boundary, because the temperature gradient is much steeper inside the LCFS than in the ergodic layer and the inflection temperature is ~ 100 eV (sample $T_{\rm e}$ profiles can be found in Refs. [22] and [24]). Note that $\langle n_{\rm e}\rangle$ in this study is calculated inside $\rho_{100\,\rm eV}$. During the feedback phase, $\rho_{100\,\rm eV}$ is slightly larger than 1, indicating that the hot plasma is fully expanding to the LCFS. In the massive gas puff phase, the hot plasma

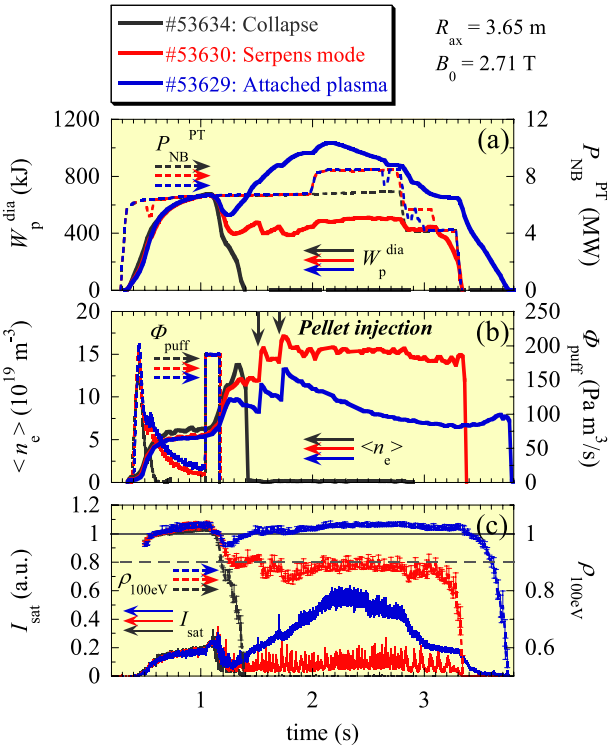

Fig. 1 Typical waveforms in the "Serpens mode" (red), "Attached plasma" (blue), and "Collapse" (gray) discharges, where (a) the magnetically measured plasma stored energy, $W_{\rm p}^{\rm dia}$, and the NB port-through power, $P_{\rm NB}^{\rm PT}$, (b) the volume averaged electron density, $\langle n_{\rm e}\rangle$, and the hydrogen flow rate of gas puffing, $\Phi_{\rm puff}$, (c) the ion saturation current measured on one of the divertor tiles, $I_{\rm sat}$, and the effective hot plasma boundary, $\rho_{100\,\rm eV}$, are shown from top to bottom. Two fueling hydrogen ice pellets are injected at t = 1.5 s and 1.7 s, in "Serpens mode" and "Attached plasma" cases.

column shrinks and $\rho_{100\,\mathrm{eV}}$ decreases below 1 due to the edge cooling effect. Also in Fig. 1 (c), the total ion saturation current measured on one of the divertor tiles, I_{sat}, is shown. When $\rho_{100\,\mathrm{eV}}$ becomes less than 1, I_{sat} significantly decreases, indicating that complete detachment is occurring, as was shown in Refs. [22–24]. Different results follow in the three discharges depending on $\langle n_{\mathrm{e}} \rangle$ in the feedback phase, i.e. reattachment, transition to the Serpens mode, and radiative collapse. Reattachment after a short period of complete detachment takes place and I_{sat} begins to increase again in the "Attached plasma" case. Fluctuations appear in I_{sat} during the Serpens mode phase. This corresponds to the rotation of a radiation belt, named the serpent [25], which will be reviewed in the next subsection.

Two fueling hydrogen ice pellets [30–32] are injected to "Serpens mode" and "Attached plasma" discharges shown in Fig. 1. In the "Attached plasma" case, $\langle n_{\mathrm{e}} \rangle$ decreases after each of two pellet injections. It is ordinarily observed that the density decays if the gas puffing and/or recycling are not enough to sustain the density. In the "Serpens mode" case, on the other hand, the density decay rate is largely mitigated and $\langle n_{\mathrm{e}} \rangle$ is increased stepwise by the pellets. Recycling in the Serpens mode is much smaller compared with the attached phase, as seen in I_{sat} (other indications of low recycling are also observed in the neutral pressure and H_α signals [22–24]). Since the high-density is sustained by the reduced recycling, the fueling efficiency for the recycling neutrals and/or the particle confinement should have been improved in the Serpens mode. This improvement might be attributed to the low temperature nature in the nested magnetic surface region below the LCFS [24]. In such a case, neutral particles penetrate inside the LCFS and be ionized. These particles are confined longer than the particles ionized in the ergodic layer, where transport parallel to the field lines connected to the plasma facing components is the main loss channel. It is apparent from Fig. 1 that a high-density flattop is easily achieved in the Serpens mode discharge, compared with the attached discharge.

2.2 Serpent and hydrogen volume recombination

As seen in Fig. 1, fluctuations appear in I_{sat} during the Serpens mode phase. Each of the peaks in the fluctuating I_{sat} appears when the serpent passes through the field of view of the diagnostics. The serpent is a helical radiation belt moving in both the poloidal and toroidal directions. Poloidal motion of the serpent is clearly seen in the temporal evolution of the radiation profile measured by an AXUV (absolute extreme ultraviolet) photodiode array [25,33] as shown in Fig. 2. The poloidal rotation speed of the serpent increases with the heating power. For example, the serpent rotates poloidally 7 times from $t = 1.41$ s to 1.76 s in the case of $P_{\mathrm{NB}}^{\mathrm{PT}} \sim 9.4$ MW, while in the case

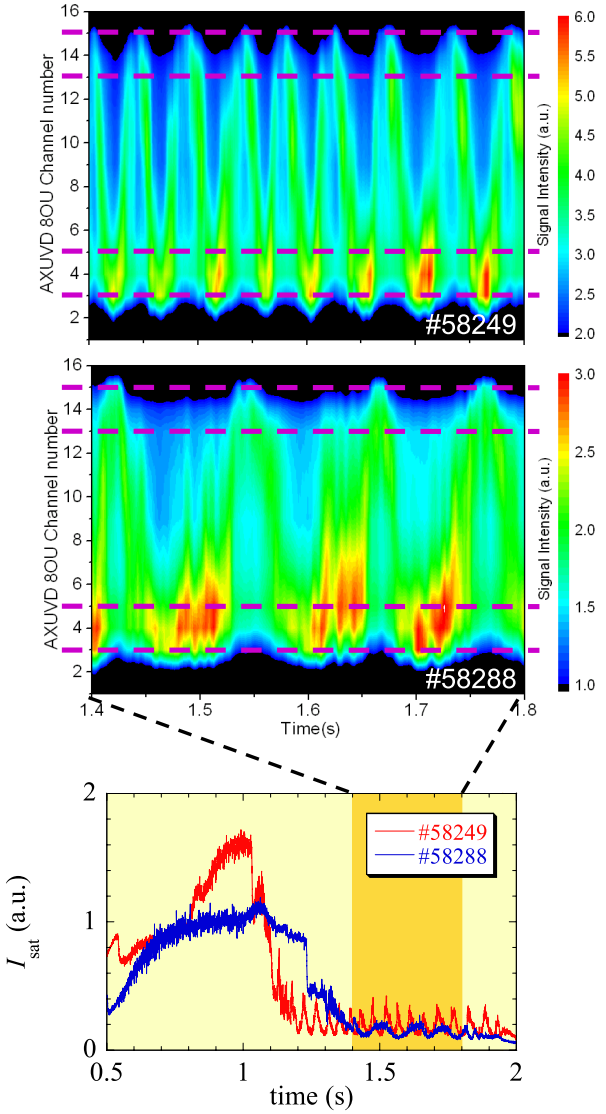

Fig. 2 The serpents observed in the temporal evolutions of the radiation profile measured by AXUV photodiode array. The poloidal rotation speed of the serpent increases and is higher in the case of $P_{\mathrm{NB}}^{\mathrm{PT}} \sim 9.4$ MW (#58249, upper contour) than in the case of $P_{\mathrm{NB}}^{\mathrm{PT}} \sim 3.9$ MW (#58288, lower contour). Horizontal broken lines denote the turning points of bright signal region, which roughly correspond to $\rho = 0.9$–1.0. The ion saturation currents in the corresponding discharges are shown in the bottom figure.

of $P_{\mathrm{NB}}^{\mathrm{PT}} \sim 3.9$ MW, it rotates only 3 times during the same period. The turning point of the bright signal (channel number of 3–5 and 13–15, see Ref. [33] for measurement details) suggests that the radial position of the serpent is within $\rho = 0.9$–1.0 [25].

In the peripheral region of the detached plasmas, volume recombination of hydrogen ions takes place due to the low electron temperature there. For instance, it was reported from W7-AS that volume recombination in the vicinity of the divertor target tiles was observed during the detached phase [34]. Furthermore, the Marfe radi-

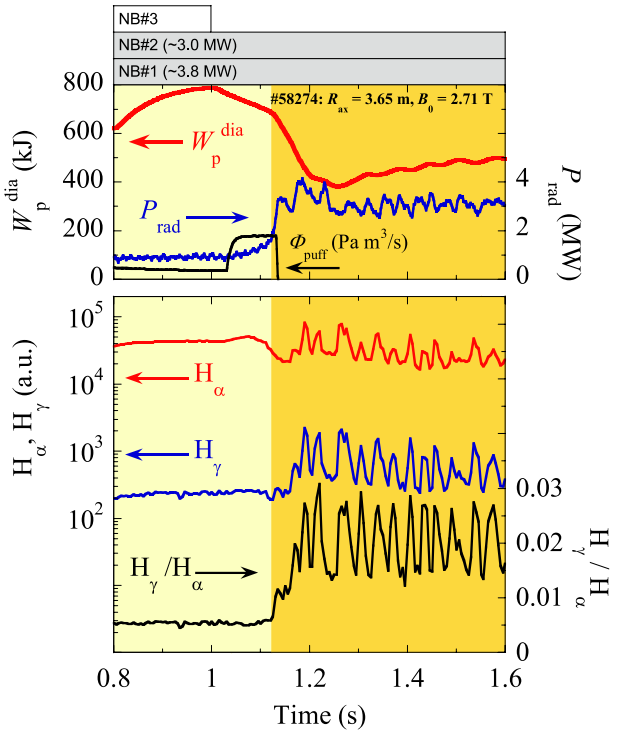

Fig. 3 Close up waveforms from a Serpens mode discharge, where the magnetically measured plasma stored energy, W_p^{dia}, the total radiation loss, P_{rad}, and the hydrogen flow rate of gas puffing, Φ_{puff}, are shown in the top figure, while H_α and H_γ intensities together with the ratio of H_γ/H_α are shown in the lower figure. The H_γ/H_α ratio increases from 0.005 in the attached phase ($t < 1.1$ s) to 0.015–0.03 in the Serpens mode phase ($t > 1.1$ s), as expected in volume recombining plasmas. Each of the peaks in H_α, H_γ, and H_γ/H_α appears simultaneously at the timings when the serpent passes through the field of view of the measurement.

ation belt observed in W7-AS was composed of strong hydrogen emission surrounded by a thin carbon emission layer [12–14]. Inside the Marfe radiation belt, the intensity ratio of H_γ/H_α was large (2–3), suggesting volume recombination [12]. A clear Balmer series is also observed in the Serpens mode. The H_α and H_γ intensities in a Serpens mode discharge are shown in Fig. 3. Fluctuations are recognized in both H_α and H_γ signals during the Serpens mode phase ($t > 1.1$ s), reflecting the rotation of the serpent. The ratio of H_γ/H_α during the Serpens mode phase is 3 – 6 times larger than that at the attached phase ($t < 1$ s). This ratio is similar to, or larger than that observed on the detached divertor target and in the Marfe radiation belt in W7-AS. Therefore, hydrogen recombination is occurring in the Serpens plasmas. The ratio of H_γ/H_α is also fluctuating with the H_α and H_γ signals and the peaks appear at the same time. This suggests that the hydrogen volume recombination is enhanced in the serpent. At this point, the serpent in LHD and the Marfe radiation belt in W7-AS resemble each other.

Volume recombination might be playing an important role in the particle balance of the detached plasmas. Ionized particles are lost in the volume recombination region and resultant neutral particles easily reenter the region inside the LCFS, and become re-ionized. In this case, the particle absorption by the plasma facing components becomes smaller compared with the attached cases (note that a small amount of the divertor flux corresponding to ~ 10 % of the attached cases still remains even at detachment and a part of the neutral particles emitted from the volume recombination region would be directly absorbed by the plasma facing components). Reduction of the number of particles absorbed in the plasma facing components (conservation of the total number of particles inside the vacuum vessel) and the improved fueling efficiency and/or the particle confinement (conservation of the number of particles inside the plasma) are the important processes to explain the particle balance and the reason why a high-density plasma is sustained in steady-state without gas puffing in the Serpens plasmas.

3. Necessary Conditions for Complete Detachment and Serpens Mode

In this section, necessary conditions to achieve complete detachment and Serpens mode are investigated. There are many candidates for the key parameters that are essential for the Serpens mode transition. Below, three typical examples are investigated to discriminate the necessity of the radiation loss, impurity emission, density ramp up rate, and gas species. It has been observed that the $m/n = 1/1$ MHD mode is destabilized at the Serpens mode, where m and n denote the poloidal and toroidal mode numbers, respectively. However, this cannot be the main mechanism triggering the Serpens mode transition, since there are discharges that do not enter the Serpens mode even though the hot plasma boundary shrinks to less than 90 % of the LCFS radius and a large fluctuation of the $m/n = 1/1$ mode is observed [22] (note that there still is a possibility that the MHD activity is playing an important role in sustaining the Serpens mode). Finally, operational regimes for complete detachment and Serpens mode are shown.

3.1 Unstable detachment

At the Serpens mode, the total radiation loss, P_{rad}, and the impurity emission such as C_{III} largely increase. However, these do not necessarily trigger the transition to the Serpens mode, as seen in the unstable detachment discharge depicted by blue lines in Fig. 4, where a Serpens mode discharge obtained under the similar experimental condition is also shown by red lines as a reference. The unstable detachment discharge does not enter the Serpens mode even though P_{rad} and the C_{III} intensity exceed the values in the Serpens mode discharge at $t = 1.7$–2.1 s. It should be noted that the dominant impurity in LHD after

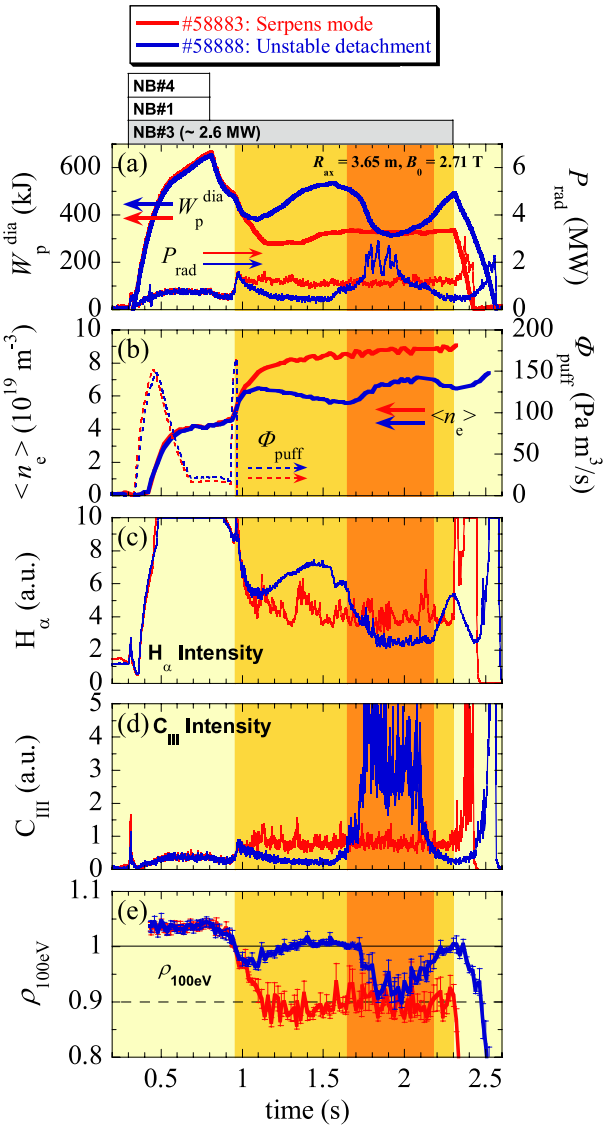

Fig. 4 Comparison of "Unstable detachment" (#58888, blue) with the "Serpens mode" (#58883, red), where (a) the magnetically measured plasma stored energy, W_p^{dia}, and the total radiation loss, P_{rad}, (b) the volume averaged electron density, $\langle n_e \rangle$, and the hydrogen flow rate of gas puffing, Φ_{puff}, (c) H_α intensity, (d) C_{III} intensity, and (e) the effective hot plasma boundary, $\rho_{100\,eV}$, are shown from top to bottom.

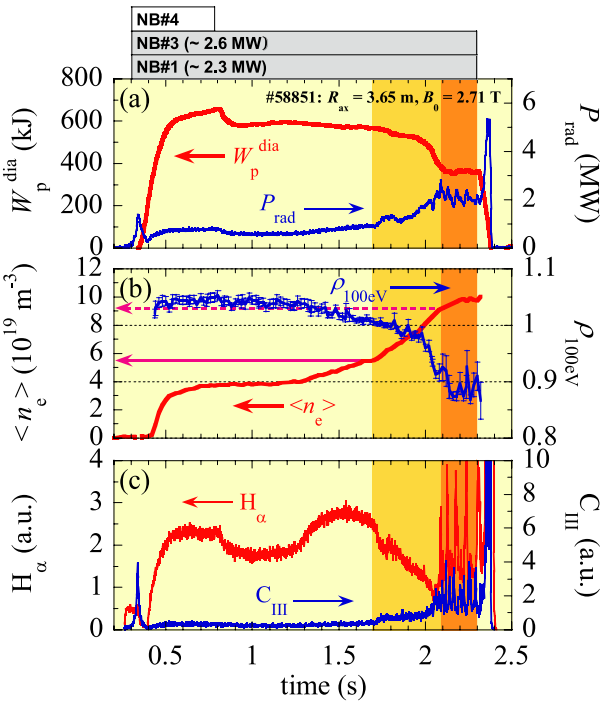

Fig. 5 Typical example of the Serpens mode transition after a slow density ramp up, where (a) the magnetically measured plasma stored energy, W_p^{dia}, and the total radiation loss, P_{rad}, (b) the volume averaged electron density, $\langle n_e \rangle$, and the effective hot plasma boundary, $\rho_{100\,eV}$, (c) H_α and C_{III} intensities, are shown from top to bottom. Transitions to complete detachment and the Serpens mode take place at $\langle n_e \rangle \sim 6 \times 10^{19}$ m^{-3} (t = 1.7 s) and $\langle n_e \rangle \sim 9 \times 10^{19}$ m^{-3} (t = 2.1 s), respectively, as indicated by horizontal arrows in (b).

the boronization [35], as in this study, is thought to be carbon ejected from the divertor tiles. In the meanwhile, $\langle n_e \rangle$ is lower in the unstable detachment discharge. The temporal behavior of P_{rad} resembles that of C_{III} [21], which is emitted at a low temperature region of less than 100 eV. This supports an assumption that the major contribution to P_{rad} is the line radiation from carbon ions in the low temperature region including the very edge region outside $\rho_{100\,eV}$. The observation that even a radiation loss of nearly 100 % ($P_{rad} \sim P_{NB}^{PT}$) cannot trigger the Serpens mode transition suggests that the parameter inside $\rho_{100\,eV}$ is more important than that outside $\rho_{100\,eV}$. Since $\langle n_e \rangle$ is calculated inside $\rho_{100\,eV}$ it is appropriate to consider a threshold of $\langle n_e \rangle$ for complete detachment and the Serpens mode.

3.2 Serpens mode by slow density ramp up

Although rapid density increase by massive gas puffing is effective for obtaining a longer high-density flattop within a limited heating pulse, it is sometimes difficult to reproduce the Serpens mode due to the variation of the wall conditioning as seen in Fig. 1. Rapid density increase is not the necessary condition since it is possible to achieve the Serpens mode with a slower density ramp up, as shown in Fig. 5. Throughout the discharge ($t < 2.3$ s), the density is feedback controlled by gas puffing of $\Phi_{puff} < 120$ Pa m^3/s. Transitions to complete detachment ($\rho_{100\,eV} < 1$) at $t \sim 1.7$ s and the Serpens mode ($\rho_{100\,eV} \sim 0.9$) at $t \sim 2.1$ s take place at similar threshold densities as the massive gas puff cases with a similar heating power of $P_{NB}^{PT} \sim 5$ MW ($\sim 6 \times 10^{19}$m^{-3} and $\sim 9 \times 10^{19}$m^{-3} for complete detachment and the Serpens mode, respectively, see Fig. 7 in Sec. 3.4). This observation emphasizes the importance of the electron density for the Serpens mode threshold.

3.3 Serpens mode with helium gas puffing

The Serpens mode experiments have been carried out mainly at a magnetic configuration of $R_{ax} = 3.65$ m, where R_{ax} denotes the major radius of the magnetic axis in the vacuum configuration. So-called inward-shifted configurations of $R_{ax} < 3.75$ m in LHD are characterized by reduced neo-classical transport compared with outward-shifted configurations of $R_{ax} > 3.75$ m [36] and the orbits of the high-energy trapped ions are well aligned with the magnetic surfaces [37]. The largest confinement volume of $\sim 30\,m^3$ is obtained at $R_{ax} = 3.6$ m. The plasma volume at $R_{ax} = 3.65$ m is similar to that at $R_{ax} = 3.6$ m and the global confinement properties are not significantly different between these two configurations. Indeed, the maximum plasma stored energy in LHD ($\sim$ 1.3 MJ, to date) has been achieved at both configurations of $R_{ax} = 3.6$ m and 3.65 m. However, it is difficult to achieve the Serpens mode by hydrogen massive gas puffing at $R_{ax} = 3.6$ m. The reasons for this and the configuration dependence of the Serpens mode have not yet been investigated.

Nonetheless, $R_{ax} = 3.65$ m is not a necessary condition for the Serpens mode. It is possible to achieve the Serpens mode at $R_{ax} = 3.6$ m, by using helium gas puffing. This also means at the same time that hydrogen gas puffing is not a necessary condition. A typical example of the helium Serpens mode discharge is shown in Fig. 6. The electron density is gradually increased by a small gas puffing of $\Phi_{puff} \leq 15\,Pa\,m^3/s$ (He). The effective fueling efficiency [38] of helium gas puffing can be larger than that of hydrogen gas puffing, because of an enhanced recycling [39]. Interestingly, transitions to complete detachment ($\rho_{100\,eV} < 1$) at $t \sim 0.9$ s and the Serpens mode ($\rho_{100\,eV} \sim 0.9$) at $t \sim 1.2$ s take place at similar threshold densities as the hydrogen gas puff case with a similar heating power (see also Fig. 5 and Fig. 7 in the next subsection). Again, this emphasizes the importance of the electron density in determining the operational regimes of complete detachment and the Serpens mode.

Although the fueling gas was helium, non-negligible amount of recycled hydrogen ions released from the vacuum vessel wall and/or the divertor tiles were included in the discharge in Fig. 6. The ratio of hydrogen ions to helium ions estimated from the recombination light observed at the end of discharge [40] ($t > 2.3$ s, just after the heating pulse) is roughly 10 %, in this case. This makes it possible to see the H_γ/H_α ratio in this discharge, as shown in the bottom of Fig. 6. Compared with the attached phase ($t < 0.9$ s), the H_γ/H_α ratio increases 3–5 times at the Serpens mode phase (t = 1.2–2.3 s). This is similar to that observed in the hydrogen Serpens mode shown in Fig. 3. Significant fluctuations are not seen in the H_α and He_I signals, but in the C_{III} and O_V signals (Fig. 6 (c)). A similar fluctuation is also seen in the H_γ/H_α ratio. This suggests the existence of the serpent and that volume recombination is enhanced in it. As in the hydrogen Serpens mode case, volume recombination might play an important role

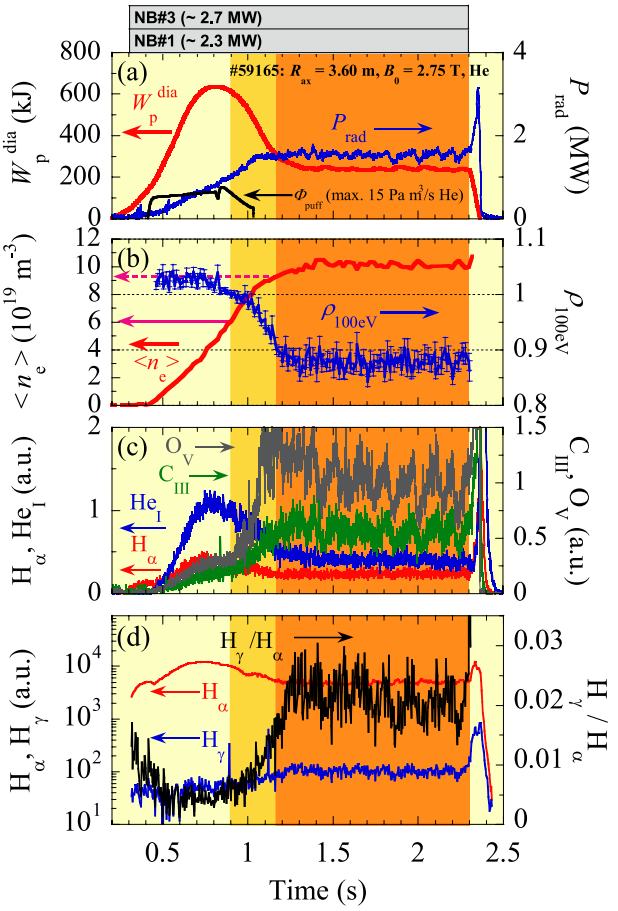

Fig. 6 Typical example of the helium Serpens mode, where (a) the magnetically measured plasma stored energy, W_p^{dia}, the total radiation loss, P_{rad}, and the flow rate of helium gas puffing, Φ_{puff} (15 Pa m^3/s He at the maximum at $t \sim 0.85$ s), (b) the volume averaged electron density, $\langle n_e \rangle$, and the effective hot plasma boundary, $\rho_{100\,eV}$, (c) H_α, He_I, C_{III} and O_V intensities, (d) H_α and H_γ intensities and the ratio of H_γ/H_α are shown from top to bottom. Transitions to complete detachment and the Serpens mode take place at $\langle n_e \rangle \sim 6 \times 10^{19}$ m^{-3} ($t = 0.9$ s) and $\langle n_e \rangle \sim 9 \times 10^{19}$ m^{-3} ($t = 1.2$ s), respectively, as indicated by horizontal arrows in (b).

in sustaining the high-density in the helium Serpens mode. However, it should be noted that enhanced recycling of helium atoms, which is implied from a smaller Φ_{puff} than the hydrogen gas puffing needed to achieve similar density, mitigates the necessity of volume recombination since the number of particles absorbed in the plasma facing components is already small in the helium plasmas.

3.4 Operational regimes for complete detachment and the Serpens mode

As has been described in the former subsections, the density is an important parameter that possibly determines the thresholds for complete detachment and the Serpens mode. In Fig. 7, summarized are the threshold densities for complete detachment (green) and the Serpens mode (pur-

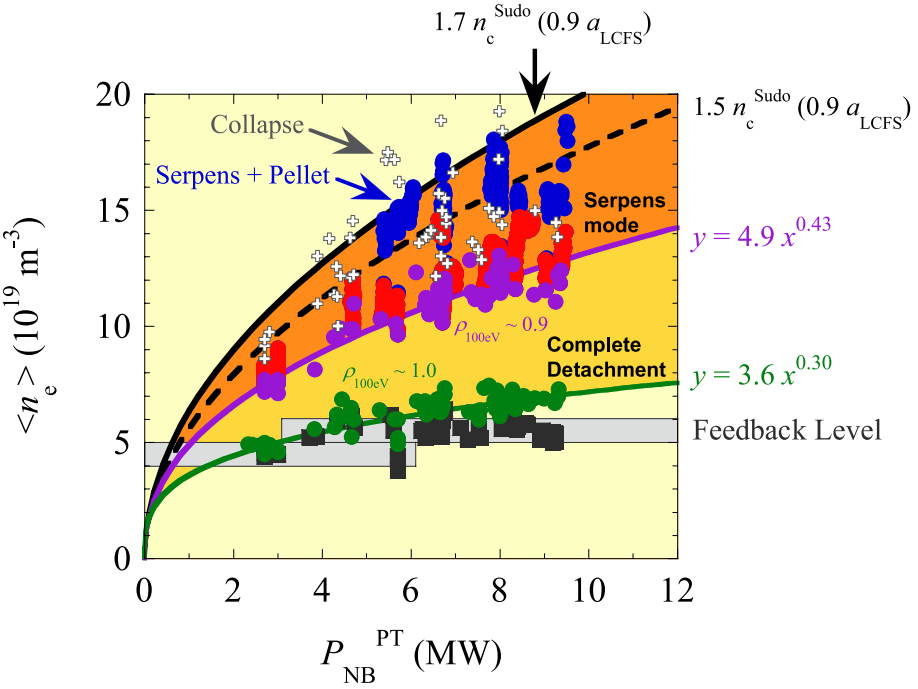

Fig. 7 Density regimes for complete detachment and the Serpens mode. Complete detachment is achieved in the region surrounded by green ($\rho_{100\,eV} \sim 1.0$) and purple ($\rho_{100\,eV} \sim 0.9$) lines. The Serpens mode is achieved in the region surrounded by purple ($\rho_{100\,eV} \sim 0.9$) and black ($1.7\,n_c^{Sudo}$ ($0.9\,a_{LCFS}$)) lines. As in Fig. 1, the discharges analyzed here are feedback controlled at their initial phases to the density denoted by "Feedback Level" (the densities achieved in the feedback phases are plotted by gray squares). Complete detachment (or the Serpens mode) takes place when $\langle n_e \rangle$ increases to that plotted by green (or purple) symbols. During the Serpens mode, $\langle n_e \rangle$ increases further due to the redistribution of the density profile from hollow to flat (red symbols), even though no further fueling is applied, and the upper envelope reaches 1.5 times as high as the Sudo limit (broken black line). By pellet injection to the Serpens plasmas (blue symbols), the upper envelope of the operational density limit is increased further to 1.7 times as high as the Sudo limit (solid black line). White crosses denote the maximum densities transiently achieved during the collapsing phase, where $\rho_{100\,eV}$ is shrinking to 0.5 – 0.8.

ple) at various P_{NB}^{PT}. These are extracted from hydrogen massive gas puff discharges. In each of the discharges, the density is initially feedback controlled to the level indicated by gray zones, as in the discharge shown in Fig. 1. After that, the density is rapidly increased by massive gas puffing. As the density increases, the hot plasma boundary shrinks and $\rho_{100\,eV}$ becomes ~ 1.0 at the density plotted by green symbols. Complete detachment takes place at this threshold density, which is fitted by $\langle n_e \rangle$ (10^{19}m^{-3}) = 3.6 (P_{NB}^{PT} (MW))$^{0.30}$ (green line). As the density increases further to the points plotted by the purple symbols, $\rho_{100\,eV}$ becomes $\sim$ 0.9. The Serpens mode appears in the density regime above this threshold density, which is fitted by $\langle n_e \rangle$ (10^{19} m^{-3}) = 4.9 (P_{NB}^{PT} (MW))$^{0.43}$ (purple line). It is not understood why the density thresholds show such heating power dependence. Nevertheless, it is meaningful to note again that these density thresholds are also observed in slow ramp up discharges with hydrogen (Fig. 5) and helium (Fig. 6) gas puffing at a similar heating power of $P_{NB}^{PT} \sim 5$ MW.

The density gradually increases during the Serpens mode due to a redistribution of the density profile from hollow to flat [24], as long as no further fueling is applied (red symbols). The upper envelope of the Serpens mode data without pellet fueling (red) reaches 1.5 times as high as the Sudo density limit [41], n_c^{Sudo} ($0.9\,a_{LCFS}$) (= $2.5(P_{NB}^{PT} B_0/((0.9\,a_{LCFS})^2 R_{ax}))^{0.5}$), where the reduced minor radius of the Serpens plasmas is approximated by $0.9\,a_{LCFS}$, and the units of n_c^{Sudo}, P_{NB}^{PT}, B_0 (magnetic field strength on the magnetic axis), a_{LCFS} and R_{ax} are 10^{19} m^{-3}, MW, T, m and m, respectively. This is comparable to that reported in the former study of 1.6 n_c^{Sudo} for attached plasmas with pellet injection, but not necessarily in steady state [21]. As shown in Fig. 1, the density of the Serpens plasmas increases stepwise after pellet injection and is sustained in steady state. Blue symbols in Fig. 7 are the data of Serpens plasmas with pellet injection. The upper envelope in this case reaches 1.7 times as high as the Sudo density limit. The "Serpens mode" discharge shown in Fig. 1 is a typical example that reaches the upper envelope.

As a reference, the maximum densities transiently achieved during the radiative collapse are also plotted by white crosses. These are obtained during the shrinking phase where $\rho_{100\,eV} \sim$ 0.5–0.8. At least two reasons lead to radiative collapse, i.e. one is excess of gas puffing (as in "Collapse" discharge in Fig. 1) and another is decrease in the heating power (as seen in "Serpens mode" discharge, at $t \sim 3.3$ s, in Fig. 1). With a help of pellet injection, the

Serpens plasmas can contain a high-density that is comparable to the collapsing plasmas, for a long time period limited only by the pulse length of the auxiliary heating.

4. Summary

Self-sustainment of a high-density flattop of over $10^{20}\,\mathrm{m}^{-3}$ is demonstrated in the Serpens mode discharges in LHD. Especially, pellet injection to the Serpens plasmas leads to a stepwise increase of the density. The intensity ratio of H_γ / H_α observed at complete detachment is larger than that in the attached phase and fluctuating with the H_α signal during the Serpens mode phase. This suggests that hydrogen volume recombination takes place at complete detachment and is enhanced in the serpent. Volume recombination is possibly playing an important role in sustaining the high density with a small amount of recycling neutrals.

The Serpens mode is achieved by using hydrogen or helium gas puffing of various flow rates from 15 to 200 Pa m^3/s (or various density ramp up rates), at $R_{\mathrm{ax}} = 3.6$ m and 3.65 m. The total radiation loss is not appropriate to determine the threshold because even a 100 % radiation loss cannot trigger the transition to the Serpens mode. The density thresholds for complete detachment and the Serpens mode are experimentally documented. Both of the threshold densities for complete detachment ($\rho_{100\,\mathrm{eV}} < 1$) and the Serpens mode ($\rho_{100\,\mathrm{eV}} \sim 0.9$) increase with heating power, i.e. the density thresholds for complete detachment and the Serpens mode are proportional to the ~ 0.3 and ~ 0.4 powers of $P_{\mathrm{NB}}^{\mathrm{PT}}$, respectively. These threshold densities are not significantly varied even under various experimental conditions.

The maximum density confined in the Serpens plasmas without further fueling is 1.5 times higher than the Sudo density limit. By applying pellet injection to the Serpens plasmas, the operational density limit in LHD, which is sustainable in steady state, has been extended to 1.7 times as high as the Sudo density limit.

Acknowledgement

This work is supported by NIFS05ULPP517 and NIFS05ULPP520.

[1] ITER-JCT and Home Teams (presented by G. Janeschitz), Plasma Phys. Control. Fusion **37**, A19 (1995).
[2] ITER Physics Expert Group on Divertor *et al.*, Nucl. Fusion **39**, 2391 (1999).
[3] A. Sagara *et al.*, Nucl. Fusion **45**, 258 (2005).
[4] C.S. Pitcher and P.C. Stangeby, Plasma Phys. Control. Fusion **39**, 779 (1997).
[5] A. Loarte *et al.*, Nucl. Fusion **38**, 331 (1998).
[6] N. Asakura *et al.*, J. Nucl. Mater. **290-293**, 825 (2001).
[7] J. Neuhauser *et al.*, Plasma Phys. Control. Fusion **37**, A37 (1995).
[8] P. Grigul *et al.*, J. Nucl. Mater. **313-316**, 1287 (2003).
[9] K. McCormick *et al.*, J. Nucl. Mater. **290-293**, 920 (2001).
[10] Y. Feng *et al.*, Nucl. Fusion **45**, 89 (2005).
[11] B. Lipschultz *et al.*, Nucl. Fusion **24**, 977 (1984).
[12] U. Wenzel *et al.*, Plasma Phys. Control. Fusion **44**, L57 (2002).
[13] H. Thomsen *et al.*, Nucl. Fusion **44**, 820 (2004).
[14] U. Wenzel *et al.*, J. Nucl. Mater. **337-339**, 196 (2005).
[15] A. Iiyoshi *et al.*, Nucl. Fusion **3**, 1245 (1999).
[16] O. Motojima *et al.*, Phys. Plasmas **6**, 1843 (1999).
[17] M. Fujiwara *et al.*, Plasma Phys. Control. Fusion **41**, B157 (1999).
[18] A. Komori *et al.*, Plasma Phys. Control. Fusion **42**, 1165 (2000).
[19] B.J. Peterson *et al.*, Phys. Plasmas **8**, 3861 (2001).
[20] Y. Xu *et al.*, Nucl. Fusion **42**, 601 (2002).
[21] B.J. Peterson *et al.*, in Fusion Energy 2004 (Proc. 20 th Int. Conf. Conf. Vilamoura, 2004) (Vienna: IAEA) CD-ROM EX/6-2 and http://www-naweb.iaea.org/napc/physics/fec/fec2004/datasets/index.html
[22] J. Miyazawa *et al.*, "Detachment Phenomena in LHD compared to W7-AS", Fusion Sci. Tech (*to appear*).
[23] J. Miyazawa *et al.*, J. Plasma Fusion Res. **81**, 331 (2005).
[24] J. Miyazawa *et al.*, Nucl. Fusion **46**, 532 (2006).
[25] S. Masuzaki *et al.*, J. Plasma Fusion Res. **81**, 649 (2005).
[26] J. Miyazawa *et al.*, J. Plasma Fusion Res. **81**, 302 (2005).
[27] J. Miyazawa *et al.*, Plasma Phys. Control. Fusion **47**, 801 (2005).
[28] J. Miyazawa *et al.*, Plasma Phys. Control. Fusion **48**, 325 (2006).
[29] K. Narihara *et al.*, Phys. Rev. Lett. **87**, 135002 (2001).
[30] H. Yamada *et al.*, Fusion Eng. Des. **49-50**, 915 (2000).
[31] H. Yamada *et al.*, Fusion Eng. Des. **69**, 11 (2003).
[32] R. Sakamoto *et al.*, Nucl. Fusion **41**, 381 (2001).
[33] B.J. Peterson *et al.*, Plasma Phys. Control. Fusion **45**, 1167 (2003).
[34] N. Ramasubramanian *et al.*, Nucl. Fusion **44**, 992 (2004).
[35] K. Nishimura *et al.*, J. Plasma Fusion Res. **79**, 1216 (2003).
[36] S. Murakami *et al.*, Plasma Phys. Control. Fusion **42**, L19 (2002).
[37] S. Murakami *et al.*, J. Plasma Fusion Res. SERIES **5**, 620 (2002).
[38] J. Miyazawa *et al.*, J. Nucl. Mater. **313-316**, 534 (2003).
[39] J. Miyazawa *et al.*, Nucl. Fusion **44**, 154 (2004).
[40] M. Goto *et al.*, Phys. Plasmas **10**, 1402 (2003).
[41] S. Sudo *et al.*, Nucl. Fusion **30**, 11 (1990).